

## Fabrication of porous alumina on quartz crystal microbalances

R. J. Lazarowich<sup>a)</sup> and P. Taborek

*Department of Physics and Astronomy, University of California, Irvine, California 92697*

B.-Y. Yoo and N. V. Myung

*Department of Chemical and Environmental Engineering, University of California, Riverside, California 92521*

(Received 19 December 2006; accepted 9 March 2007; published online 25 May 2007)

Nanoporous alumina structures were fabricated on quartz crystal microbalances (QCMs) by electrochemically anodizing aluminum electrodes which had a typical thickness of 13  $\mu\text{m}$ . By varying the temperature and voltage of anodization, the diameter of the cylindrical pores could be controlled in the range of 12–40 nm. Properties of the porous films were determined from scanning electron microscopy images and by analyzing isotherms of nitrogen, propane, and water. The isotherms showed signatures of capillary condensation and hysteresis. The mass sensitivity of the QCMs with porous alumina electrodes was increased by a factor of up to 120 compared to conventional QCMs with flat electrodes. Measurements at atmospheric pressure and room temperature in which the relative humidity was varied showed that QCMs with porous alumina electrodes are very sensitive to the partial pressure of water, and can be used as humidity sensors.

© 2007 American Institute of Physics. [DOI: [10.1063/1.2730563](https://doi.org/10.1063/1.2730563)]

### I. INTRODUCTION

Quartz crystal microbalances (QCMs) are round quartz disks approximately 1 mm in thickness and 15 mm wide that oscillate in the shear mode with high mechanical quality factor ( $Q$ ). Thin film metallic electrodes on the flat surfaces of the quartz allow the shear vibration to be driven and detected electronically. If a film is condensed onto the surfaces of the microbalance, the added mass decreases the resonant frequency, which can be measured to high precision because of the high  $Q$ . The mass of adsorbed liquids can also be detected as long as the film thickness is small compared to the viscous penetration depth  $\delta = \sqrt{\eta / \pi \nu \rho}$ , where  $\eta$  and  $\rho$  are the viscosity and density of the liquid, and  $\nu$  is the frequency of the QCM.<sup>1</sup> For a low viscosity fluid such as water,  $\delta = 250$  nm. Conventional QCMs have nominally flat metallic electrodes. The resonant frequency is sensitive not only to the mass but also to parasitic effects such as temperature and pressure changes and viscous coupling to the surrounding vapor. The mass sensitivity of the QCM can be increased<sup>2</sup> and the coupling to the adsorbed film<sup>3</sup> can be altered by using porous electrodes. In addition to having a high surface area, useful porous electrodes must also be rigidly bonded to the QCM surface so that the high  $Q$  can be maintained. At least three types of porous materials have been recently used to enhance the sensitivity of QCMs: porous gold,<sup>2,4</sup>  $\text{CaF}_2$ ,<sup>4,5</sup> and porous alumina.<sup>3</sup> Porous alumina has the potential advantage that the orientation and geometry of the pores are very uniform and the pore size can be controlled by the fabrication process. Although processes for making anodized alumina have been known for nearly 60 years,<sup>6</sup> there has been recent renewed interest in this material for potential applications to nanotechnology.<sup>7,8</sup> Most work on anodized alumina has focused on forming freestanding films starting

from aluminum foils. For QCM applications, it is more convenient to anodize an aluminum film that has been deposited on the quartz, but much less work has been done on anodization of thin aluminum films on a substrate. In Sec. II, we describe our fabrication process, which utilized a three step etch and anodization process on 13  $\mu\text{m}$  thick aluminum films, and resulted in highly uniform independent cylindrical pores with the axis perpendicular to the mode of oscillation. In Sec. III, we describe forward and reverse adsorption isotherms using  $\text{N}_2$  at 77 K and water and propane near room temperature. The isotherms show signatures of capillary condensation and hysteresis. These features can be used to characterize the porous electrodes, as discussed in Sec. IV. Finally, the application of a porous alumina electrode for a humidity sensor is discussed in Sec. V.

### II. FABRICATION OF SAMPLES

SC-cut quartz wafers of 14 mm in diameter and 0.33 mm in thickness were used as a basis for the QCMs. The initial electrodes were approximately 13  $\mu\text{m}$  aluminum films e-beam evaporated onto each side of the quartz disk in a keyhole pattern with a central diameter of 6 mm. The wafers were placed in a standard HC-43 package with long wires soldered to the leads. In order to clearly define the region of anodization, the entire QCM and the holder except for the central region of the Al electrodes were coated with Microstop™ lacquer using a paintbrush. The Microstop™ is impervious to acid and can be conveniently removed with acetone upon completion of the process.

0.3M oxalic acid was used as the electrolyte for anodization. A custom electrode holder allowed the microbalance to be completely submersed in the acid between two graphite sheets, 1/8 inches in thickness, which were used as the cathodes. Using this setup, the Al electrodes on both sides of the QCM could be anodized simultaneously. The anodization

<sup>a)</sup>Electronic mail: rlazarowich@gmail.com

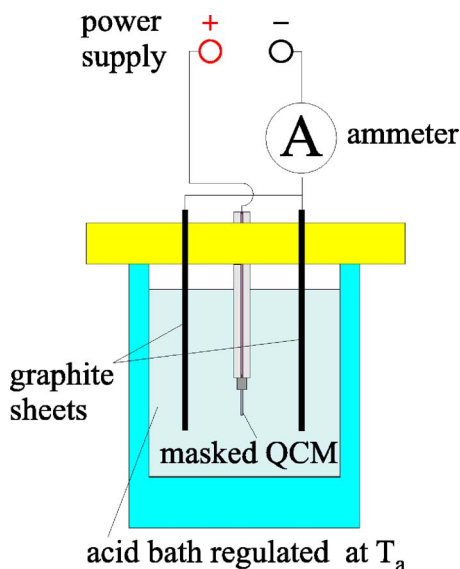


FIG. 1. (Color online) A schematic of the setup operated to electrochemically anodize aluminum films is drawn. The jacketed beaker is filled with 0.3M oxalic acid that is regulated at  $T_a$  using chilled water that circulates through its lining from a proportional-integral-derivative (PID)-controlled chiller. The bath is stirred using a magnetic stirrer. The anodization potential is provided by a dc power supply while an ammeter is used to monitor the current density.

process is very sensitive to temperature, so it was carried out in a double walled beaker using thermally regulated chilled water to stabilize the temperature. The anodization apparatus and circuit components are shown in Fig. 1.

Previous work on anodization of Al foils has shown that a highly regular pore structure can be generated using a three step anodize-etch-anodize process;<sup>9</sup> we have adapted this process for use on thin Al films. The first step consisted of anodization in the oxalic acid bath for a length of time needed to anodize the top 1–3  $\mu\text{m}$  of the aluminum film, which was usually less than 30 min. Then, the sample was placed in a solution of 4 wt %  $\text{CrO}_3$  and 10 vol %  $\text{H}_3\text{PO}_4$  for 14 h. The pores, once initiated, were much narrower near the surface compared to just below the surface, where they were both wider and more uniform. This intermediate etching removed the surface region where the pores were narrowed resulting in pores that were of uniform diameter throughout the length of the pore. In the final step, the wafer was anodized for 0.5–7 h, depending on current density, which increased exponentially with anodizing voltage as shown in Fig. 2. The Al films were anodized for a time shorter than required to completely anodize them, thereby leaving a conductive film under the porous structure for electronic conduction. The value of  $\nu_0$  with the 13  $\mu\text{m}$  Al films was 5.2 MHz, and after the anodization process was complete, this increased to roughly 5.25 MHz due to mass loss during etching. Figure 3 shows that following the fabrication process, QCMs with porous alumina electrodes retain a  $Q$  of  $2.5 \times 10^4$ . The highest values of  $Q$  are retained when either a very thin conductive film ( $< 2 \mu\text{m}$ ) is left under the porous alumina, or when a very thin anodized film is applied. On samples where the thickness of the porous film and remaining aluminum are similar, the quality factor decreases up to a factor of 4.

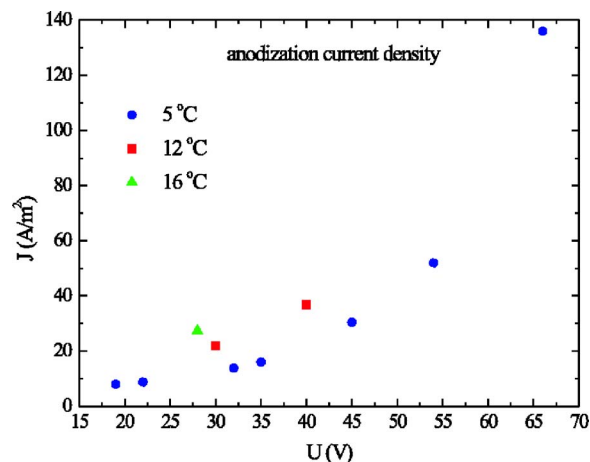


FIG. 2. (Color online) Current density  $J$  during anodization as a function of the anodization potential  $U$  for several temperatures. The area of the exposed aluminum  $A_a$  is approximately  $0.52 \text{ cm}^2$ .

A growth rate equation for the pore length  $h$  can be derived by using the number of electrons exchanged from the aluminum work piece (anode) towards the graphite (cathode). During anodization, aluminum atoms are triply oxidized to produce  $\text{Al}^{3+}$  cations that then react with the oxygen anions from the electrolyte to create  $\text{Al}_2\text{O}_3$ . The total number of electrons freed at the anode  $n_{\text{an}}$  is represented by

$$n_{\text{an}} = 3 \left( \frac{\rho_{\text{Al}} A_a h}{m_{\text{Al}}} \right), \quad (1)$$

where  $\rho_{\text{Al}}$  is the bulk density of aluminum,  $m_{\text{Al}}$  is the mass of one aluminum atom, and  $A_a$  is the exposed anodization area. At the beginning of the first anodization step, the current  $I$  is relatively high as a barrier layer forms, which quickly drops as the layer becomes an insulator, but increases to a constant value after pores nucleate. In the second step, after an initial rise, the current decreases to the same constant value. Notably, in both cases, a steady-state value is reached within 2 min, a time negligible to the total anodization time  $\tau$ . Therefore, the total charge transported to the cathode can be

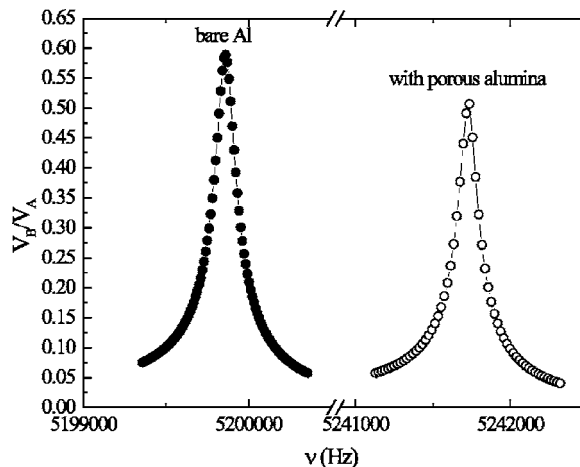


FIG. 3. Resonance plots in vacuum of QCMs before and after the fabrication process are shown. The quality factor  $Q$  decreases slightly from  $3 \times 10^4$  to  $2.5 \times 10^4$ .

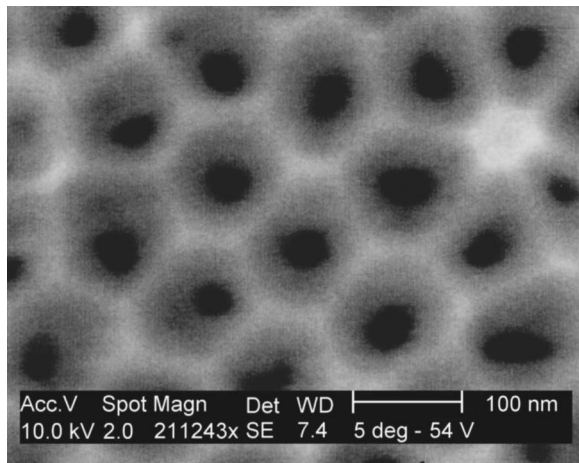


FIG. 4. SEM image of the top surface of a porous alumina fabricated on a QCM. The anodization temperature was 5 °C and the voltage was 54 V. The diameter of the pores is in good agreement with the values given in Table I.

estimated from the current  $I$  with the number of electrons collected  $n_{\text{cat}}$  over a period of time  $\tau$  being

$$n_{\text{cat}} = \frac{I\tau}{e}, \quad (2)$$

where  $e$  is the value of fundamental charge,  $1.602 \times 10^{-19}$  C. The growth rate  $\dot{h}(\tau)$  is obtained by assuming a conservation of electrons in the system leading to

$$\dot{h}(\tau) = \frac{m_{\text{Al}}J}{3e\rho_{\text{Al}}}, \quad (3)$$

where  $J$  is the current density,  $I/A_a$ . For the samples created in this report, the total number of electrons transferred was on the order of  $10^{20}$  for complete anodization of the aluminum, which is consistent with the amount of electrons available in the original film. Growth rates of 1.3–5  $\mu\text{m}/\text{h}$  are calculated with current density values from Fig. 2 in the region where uniform samples were fabricated.

The final result of the process described above was a metallic aluminum film (thickness range of 1–8  $\mu\text{m}$ ), which served as the electrode for the QCM with an anodized porous overlayer (thickness range of 1–12  $\mu\text{m}$ ) which consisted of a quasiperiodic array of approximately cylindrical pores which were perpendicular to the plane of the film. Figure 4 is a scanning electron microscopy (SEM) image of the top surface of the anodized layer which shows the cell structure and the openings of the cylindrical pores, while Fig. 5 is an image of a cross section of the anodized layer which was made visible by cracking a QCM in half and shows well aligned nonintersecting pores. The pore density depended primarily on the anodization potential and ranged from approximately 350 pores/ $\mu\text{m}^2$  at  $U=20$  V to less than 100 pores/ $\mu\text{m}^2$  at  $U=50$  V. The pore diameter was dependent on both temperature and the anodization potential, with larger potentials leading to larger pore diameters until the voltage reached approximately 50 V. For larger anodization potentials, the growth mode switched from a single pore per cell to several smaller pores per hexagonal cell, as shown in Fig. 6.

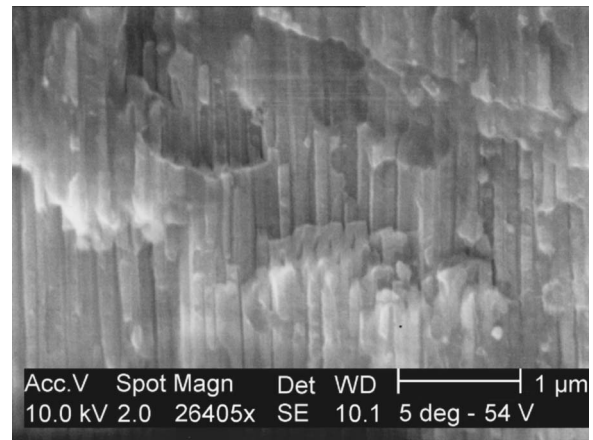


FIG. 5. SEM image of a cross section of porous alumina film grown on a QCM. The QCM was cracked in half to obtain this image, which shows parallel nonintersecting cylindrical pores oriented perpendicular to the substrate.

Although all the samples presented here were anodized using oxalic acid, attempts were also made to anodize using another common electrolyte, sulfuric acid.<sup>7,9-11</sup> However, for the same range of anodization voltages as used with oxalic acid, the current density was much larger in sulfuric acid. With the potentials set at values high enough to create a porous substrate, the high  $J$  values caused rapid anodization of the film and fully anodized a film in a very short time. Therefore, the use of sulfuric acid was abandoned because it became impossible to do the desired three step process for our Al films with 13  $\mu\text{m}$  thickness.

### III. ISOTHERMS

The fabricated samples were mounted inside a copper cell equipped with electrical feedthroughs and a fill line that was attached to a vacuum pump and gas handling system. Nitrogen isotherms were performed with the cell in a pressure regulated bath of liquid nitrogen. Propane and water isotherms were done with the cell in a temperature controlled water bath. Forward and reverse isotherms were collected by

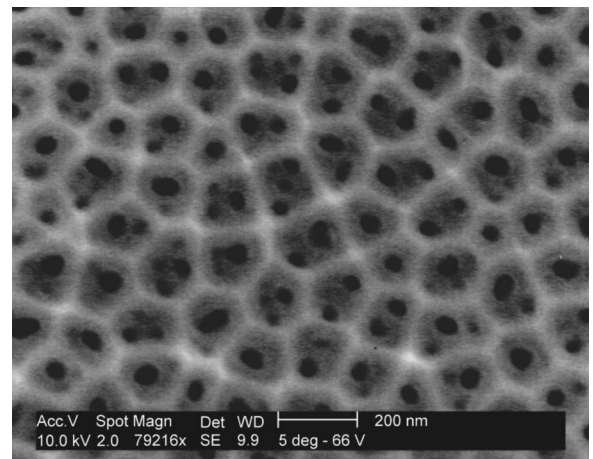


FIG. 6. SEM image of porous alumina anodized at 66 V. At this voltage, a significant number of cells contain multiple small diameter pores rather than a single large diameter pore. The nonuniform pore size distribution complicates the analysis for this type of material.

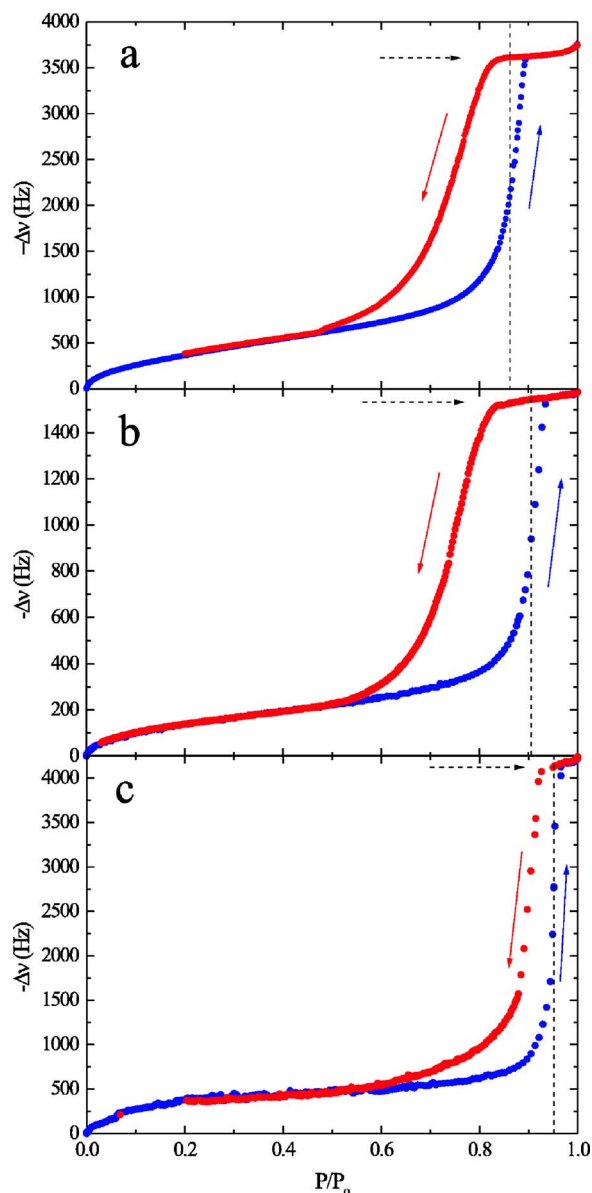


FIG. 7. (Color online) Forward and reverse nitrogen isotherms at  $T=77$  K as a function of the reduced pressure  $P/P_0$  for samples anodized at  $5^\circ\text{C}$  at three different voltages. The capillary condensation point which is determined by the steepest portion of the forward isotherm is marked with a vertical dashed line. The frequency shift  $\Delta\nu_V$  corresponding to full pores is marked with a horizontal dashed arrow. As described in the text, these features are used to determine the pore diameter and length. (a) Anodization voltage  $U=22$  V and pore diameter  $d=15$  nm; (b)  $U=32$  V,  $d=20$  nm; and (c)  $U=54$  V,  $d=40$  nm. This series of isotherms shows direct correlation between the increase of anodizing potential and pore diameter.

monitoring the resonance frequency as the cell was either dosed with vapor or had vapor removed from it. The frequency shift  $\Delta\nu$  due to a change in adsorbed mass  $\Delta m$  is given by

$$\Delta\nu = \left( -\frac{2\nu_0^2}{nZA_e} \right) \Delta m, \quad (4)$$

where  $n$  describes the harmonic of the oscillation mode,  $Z$  is the acoustic impedance, and  $A_e$  is the geometrical area of an electrode. Values of these parameters for the QCMs used in this experiment are  $Z=9\,507\,260$   $\text{kg}(\text{m}^2\text{s})^{-1}$ ,  $A_e=0.28$   $\text{cm}^2$ ,

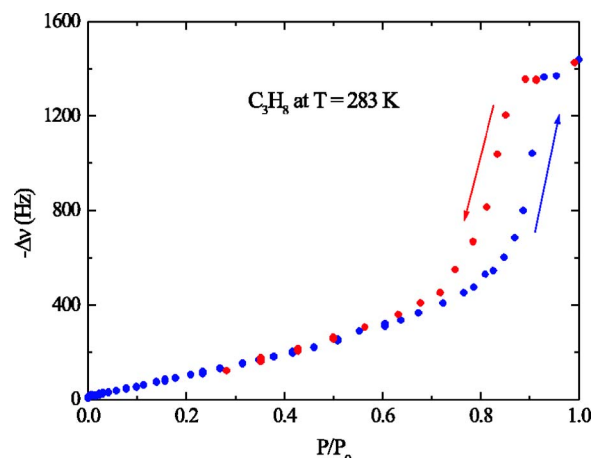


FIG. 8. (Color online) Forward and reverse isotherms of propane ( $\text{C}_3\text{H}_8$ ) on a QCM with porous alumina electrodes at  $T=283$  K. The porous alumina was anodized at  $T_a=12^\circ\text{C}$  at a voltage of 30 V. The saturated vapor pressure  $P_0$  for propane at this temperature is 6.34 bars.

and  $n=1$ ; further details are discussed in Ref. 4.

Nitrogen isotherms at 77 K for samples anodized at three different voltages,  $U=22$ , 32, and 54 V, are shown in Fig. 7. In general, the interaction between  $\text{N}_2$  and the substrate is relatively weak and isotherms resemble those as seen on  $\gamma$  alumina, but contain H1 hysteresis loops characteristic of cylindrical pores,<sup>12</sup> as expected based on the SEM images. The reduced pressure value at which capillary condensation takes place on the forward branch,  $(P/P_0)_c$ , is marked with a vertical dashed line. The capillary condensation point systematically moves to higher pressures as the anodization voltage is increased, which is consistent with the picture that the pore diameter increases with anodization voltage in this range.

Although nitrogen isotherms are most often used to deduce structural properties, we have also tested the response of our devices using water and propane, which span a wide range of chemical properties and vapor pressure. Figure 8 shows an isotherm for propane at  $T=283$  K. The isotherm has qualitatively the same features of hysteresis and closure at a pressure below the saturated vapor pressure, which in this case is above 6 atm.. Figure 9 shows an isotherm of water at  $T=281$  K; the saturated vapor pressure at this temperature is 8.3 Torr. Water is a polar fluid that interacts strongly with itself and does not wet most solid materials. It nevertheless undergoes capillary condensation in the porous alumina.

#### IV. STRUCTURAL PROPERTIES

Isotherms such as those in Fig. 7 which show capillary condensation can be analyzed in a number of ways to obtain structural information about the pores, which are typically assumed to be cylindrical. For small values of the reduced pressure  $P/P_0$ , a film of thickness  $t$  forms on the inside walls of the cylinders, while the central region of the pore is filled with vapor, and has a radius  $r$ . At a sufficiently high value of  $P/P_0$ , the liquid film becomes unstable and the pore fills with liquid; this point is indicated by the vertical dashed

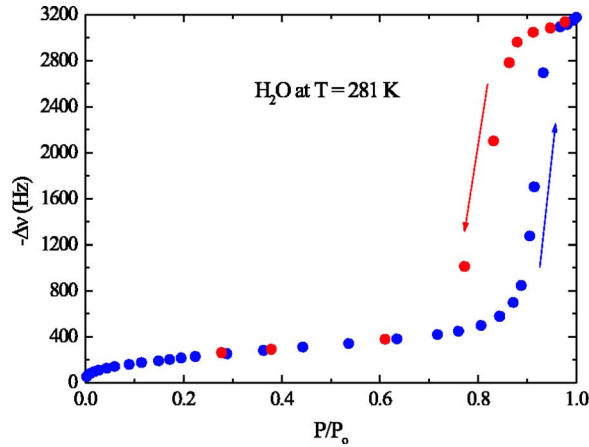


FIG. 9. (Color online) Forward and reverse isotherms of  $\text{H}_2\text{O}$  on a QCM with porous alumina electrodes at  $T=281$  K. The saturated vapor pressure  $P_0$  of water at this temperature is 8.3 Torr.

lines in Fig. 7. Previous work has shown that for  $\text{N}_2$ , the relation between the film thickness  $t$  and the reduced pressure  $P/P_0$  is

$$\ln\left(\frac{P}{P_0}\right) = -\frac{16.11}{t^2} + 0.1682e^{-0.1137t}, \quad (5)$$

where  $t$  is in units of angstroms.<sup>13</sup> At the initial point of capillary condensation, liquid and vapor coexist in the pore with a hemispherical meniscus separating them. The curved interface implies that the pressure in the liquid is lower than in the vapor. The Kelvin equation

$$r = -\frac{2v_m\sigma_{lg}}{RT \ln(P/P_0)_c} \quad (6)$$

is a thermodynamic relation between the meniscus radius  $r$  the liquid vapor surface tension  $\sigma_{lg}$ , the liquid molar volume  $v_m$ , and the reduced pressure of capillary condensation onset  $(P/P_0)_c$ . The meniscus radius  $r$  and the film thickness  $t$  can be combined to estimate the pore diameter  $d_1$  at  $(P/P_0)_c$  using

$$d_1 = 2(t + r). \quad (7)$$

The surface area of the pores  $A_s$  was measured using standard Brunauer-Emmett-Teller (BET) analysis of  $\text{N}_2$  isotherms at 77 K on the range of  $0.08 < P/P_0 < 0.30$ .<sup>14</sup> For reference, identical analysis on a QCM with flat Al electrodes resulted in  $0.63 \text{ cm}^2$  of surface area. The total pore volume  $V_p$  was estimated from the frequency deflection at the closure point of the hysteresis loop  $\Delta\nu_V$ , marked by vertical dashed arrows in Fig. 7, using the relation

$$V_p = \frac{(\Delta\nu_V)ZA_e}{2\nu_0^2\rho}. \quad (8)$$

Using the assumption of cylindrical pores, the surface area and volume measurements can be combined to form another estimate of the pore diameter

$$d_2 = \frac{4V_p}{A_s}. \quad (9)$$

Table I shows this analysis done on the adsorption branch of the samples for a  $\text{N}_2$  at 77 K. The pore volumes along with  $A_s$  are given in Table I as well as a measurement of pore size using Eq. (9).

The alumina thickness, or equivalently, the pore length  $h$  can be estimated from Eq. (3). This parameter was also determined by equating the total pore volume  $V_p$  from Eq. (8) to the product of the volume per pore  $h\pi d^2$  and the total number of pores  $A_e n_p$ , where  $A_e$  is the area of the top surface of the electrode and  $n_p$  is the number density of the pores per unit area.  $h$  is given by

$$h = \frac{1}{2} \left( \frac{4V_p}{\pi d^2 n_p A_e} \right). \quad (10)$$

The extra factor of one-half is to account for the fact that the total pore volume is measured over two electrodes.  $n_p$  was determined from SEM images such as that shown in Fig. 4 by counting the number of pores within a  $500 \text{ nm} \times 500 \text{ nm}$  square. Some care is taken to compensate for partial pores within the box since the counting area is much

TABLE I. The structural properties of porous alumina samples fabricated are shown. The temperature of the anodizing bath  $T_a$  and the anodizing potential  $U$  for each sample are given in the first two columns.  $d_1$  is the pore diameter computed from Eqs. (5)–(7) using the capillary condensation onset reduced pressure  $(P/P_0)_c$  from  $\text{N}_2$  isotherms.  $A_s$  is the area of each sample determined from BET analysis.  $V_p$  is the pore volume measured from the limiting point of hysteresis loops and Eq. (8).  $d_2$  is the pore diameter determined from Eq. (9).  $n_p$  is the pore number density measured from SEM images.  $h$  is the pore length from Eq. (10).

$T_a$ (°C)	$U$ (V)	$(P/P_0)_c$	$d_1$ (nm)	$A_s$ ( $\text{cm}^2$ )	$V_p$ ( $\text{mm}^3$ )	$d_2$ (nm)	$n_p$ ( $\mu\text{m}^2$ )	$h$ ( $\mu\text{m}$ )
5	19	0.844	12.9	6.6	0.0021	12.7	392	0.71
5	22	0.867	15.2	64.2	0.0210	13.2	356	6.75
5	32	0.905	20.2	22.3	0.0094	16.8	204	2.90
5	35	0.909	21.3	8.4	0.0036	17.2	180	1.53
5	45	0.914	23.5	5.3	0.0028	21.3	96	1.62
5	54	0.951	40.9	25.0	0.0253	40.5	72	4.99
5	66	0.949	39.3	34.6	0.0322	37.2	44	6.65
12	30	0.911	22.7	29.8	0.0125	16.8	212	4.75
12	40	0.942	34.6	74.5	0.0604	32.5	120	11.66
16	28	0.917	24.3	61.8	0.0365	23.6	240	6.48

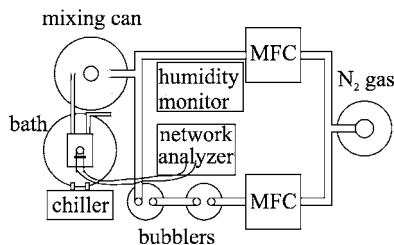


FIG. 10. Schematic of setup for constant flow measurements. The QCM is placed in a cell that is submersed in a water bath. The system is thermally regulated using a conventional chiller. Nitrogen gas passes through MFCs. The output flow of one of the MFCs goes through bubblers and then to the mixing can, while the output of the other leads straight to the mixing can. The humidity is monitored before the flow arrives in the experimental cell. The temperature of the bath is kept only slightly lower than room temperature so that there is no great difference in the humidity of the mixing can and the experimental cell.

smaller than  $A$  and a miscount could potentially cause a large error. The number density given in Table I is scaled to represent the number of pores within a square micron.  $n_p$  is also used to calculate the porosity  $\varepsilon$  of the structures,

$$\varepsilon = \left( \frac{\pi n_p d^2}{2} \right), \quad (11)$$

which is the volume fraction of pores in the material. The porosities of all the samples studied were within a range of 0.06–0.14. SEM images show that a pore encompasses about 1/7 to 1/10 of a single cell volume, depending on the sample, which also gives a good estimate of the porosity.

SEM images were also used to determine the interpore distance  $a$ . Previous work on anodization of aluminum foils has shown that  $a$  can be empirically related to the pore diameter and anodization voltage through  $a = d + 2\phi U$  where  $\phi \approx 1.4 \text{ nm/V}$ .<sup>6,15</sup> A similar relation holds for the anodization of our thin aluminum films, but with a  $\phi$  value of 0.74 nm/V. It is possible that simultaneous anodization of both electrodes causes a reduction in the thickness of the cell walls.

## V. HUMIDITY MEASUREMENTS

Previous groups have tried to implement QCMs with porous electrodes as humidity sensing devices.<sup>16</sup> Humidity measurements were obtained using the set up shown in Fig. 10. The QCM with the porous electrode was placed in a cell and submersed in a temperature regulated water bath. The cell had separate input and output gas flow lines. The flow of pressurized dry nitrogen gas from a tank was directed into two mass-flow controllers (MFC). The output of one MFC provided a source of nitrogen with 0% humidity. The output of the other MFC flowed through two bubblers at room temperature in series which produced nitrogen at 100% humidity; the two streams were mixed in the mixing can. The flow of each MFC was adjusted to achieve the desired humidity while the total flow remained near 1000 SCCM (SCCM denotes cubic centimeter per minute at STP). The relative humidity was monitored using a Vaisala HMP238 humidity and temperature transmitter.

This apparatus was first used to calibrate the response of a QCM with a flat gold electrode as a function of relative

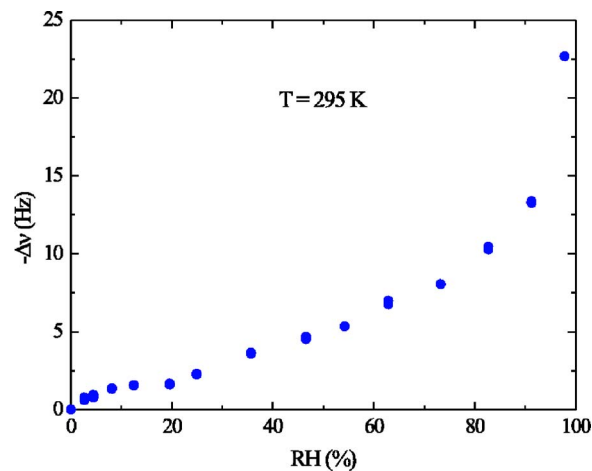


FIG. 11. (Color online) Measurement using QCM with flat Au electrodes under constant flow of  $N_2$  as relative humidity is changed at  $T=295 \text{ K}$ .

humidity. The results are shown in Fig. 11. The response is approximately linear and nonhysteretic. From Eq. (4), the expected frequency shift is 3.94 Hz per layer of liquid water. At saturation, there are approximately seven layers of water on the surface. The results of the same type of measurement with a porous alumina electrode are shown in Fig. 12. The behavior of the frequency shift as a function of relative humidity is qualitatively similar to the pure water isotherm shown in Fig. 9. Both measurements show capillary condensation and hysteretic adsorption when the degree of saturation is above approximately 80%, even though the total pressure in the two cases differ by almost a factor of 100. This shows that the nitrogen is an inert spectator, and the frequency shift of the QCM is determined by the saturation of water vapor. In the regime with  $10\% < \text{relative humidity (RH)} < 80\%$ , the response of the QCM with porous electrodes is approximately linear in RH and is larger than the flat electrode response by an amount proportional to the increase in surface area. A comparison of the frequency shift for a flat electrode QCM with porous electrode QCMs with area ratios of nearly 50 and 120 are shown in Fig. 13.

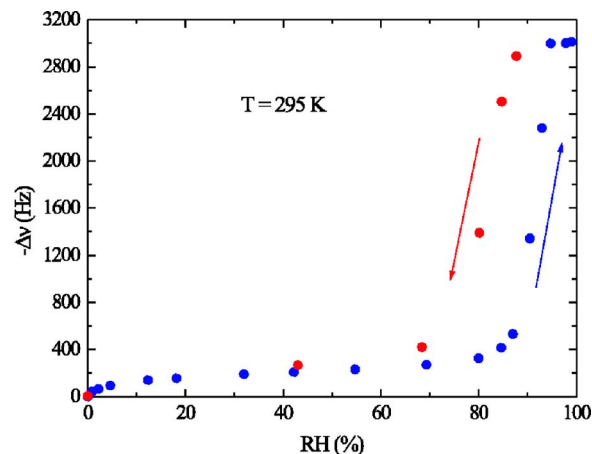


FIG. 12. (Color online) Measurement using QCM with porous alumina electrodes, fabricated at  $T_a=12^\circ \text{ C}$  and  $U=30 \text{ V}$ , under constant flow of  $N_2$  as relative humidity is changed at  $T=295 \text{ K}$ .

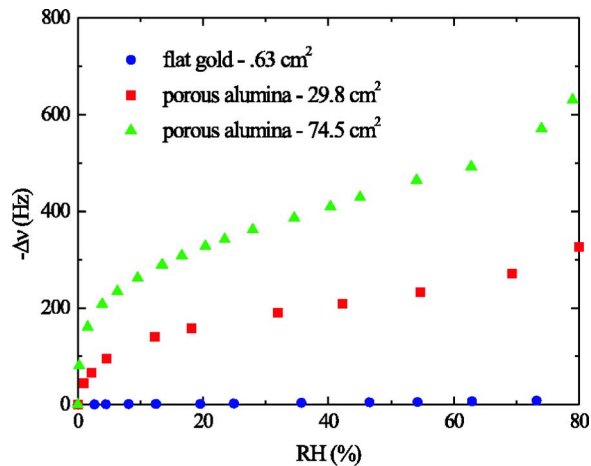


FIG. 13. (Color online) Comparison of constant flow measurements of the frequency shift  $-\Delta\nu$  for porous alumina and flat samples as a function of relative humidity (RH) at  $T=295$  K. Only the adsorption branch is shown, where the ratio of adsorbed mass is roughly the same as the ratio of surface area. One layer of water on flat electrodes causes a change in frequency of 3.94 Hz.

## VI. DISCUSSION AND CONCLUSIONS

Previous work with freestanding aluminum foils has shown that highly regular pore structure can be achieved with a three step anodize-etch-anodize process. The properties of the porous alumina are strongly affected by the choice of electrolyte and the anodization voltage and temperature. We have adapted this growth technique to form porous alumina directly on the thin film aluminum electrodes of a QCM. Although the pore structure obtained with the anodized thin films is not quite as regular as in freestanding foils, the process nevertheless produces highly oriented uniform cylindrical pores which can increase the effective adsorption area of the QCM by more than two orders of magnitude without significantly degrading  $Q$ . Adsorption isotherms on the porous electrode QCMs show the signatures of capillary condensation and hysteresis. The features of the isotherms in conjunction with SEM images provide a consistent description of the geometry of the pores. Using this type of data, we have shown that systematic variation of the process parameters lead to growth of material with a well defined pore

diameter which can be controlled in the range of approximately 10–40 nm. Experiments with nitrogen/water vapor mixtures show that the QCMs with porous alumina electrodes respond to the degree of saturation of the condensable component. The sensitivity of the humidity sensors is proportional to the area of the porous electrode, which can be 10–100 times higher than a conventional flat electrode QCM. The enhanced sensitivity lowers the threshold of detectability of an adsorbent and reduces the importance of spurious effects such as temperature and pressure fluctuations. Although we have demonstrated this sensitivity enhancement for water vapor, we expect that a high specific area QCM with high  $Q$  will be useful for other sensor applications.

## ACKNOWLEDGMENTS

The authors thank Tommy Farm at UC Riverside and Alex Jvirblis of Curtis Technology, San Diego, CA for assistance in fabricating samples. This work was supported by NSF DMR 0509685.

- <sup>1</sup>G. Sauerby, *Z. Phys.* **155**, 206 (1959).
- <sup>2</sup>M. Hieda, R. Garcia, M. Dixon, T. Daniel, D. Allara, and M. Chan, *Appl. Phys. Lett.* **84**, 628 (2004).
- <sup>3</sup>I. Goubaidoulline, J. Reuber, F. Merz, and D. Johannsmann, *J. Appl. Phys.* **98**, 014305 (2005).
- <sup>4</sup>R. J. Lazarowich and P. Taborek, *Phys. Rev. B* **74**, 024512 (2006).
- <sup>5</sup>D. R. Luhman and R. B. Hallock, *Phys. Rev. Lett.* **93**, 086106 (2004).
- <sup>6</sup>F. Keller, M. S. Hunter, and D. L. Robinson, *J. Electrochem. Soc.* **100**, 411 (1953).
- <sup>7</sup>E. C. Dickey, O. K. Varghese, K. G. Ong, D. Gong, M. Paulose, and C. A. Grimes, *Sensors* **2**, 91 (2002).
- <sup>8</sup>W. Romer and C. Steinham, *Biophys. J.* **86**, 955 (2004).
- <sup>9</sup>N. V. Myung, J. Lim, J.-P. Fleurial, M. Yun, W. West, and D. Choi, *Nanotechnology* **15**, 833 (2004).
- <sup>10</sup>A. P. Li, F. Muller, A. Birner, K. Nielsch, and U. Gösele, *J. Appl. Phys.* **84**, 6023 (1998).
- <sup>11</sup>O. Jessensky, F. Muller, and U. Gösele, *J. Electrochem. Soc.* **145**, 3735 (1998).
- <sup>12</sup>K. S. W. Sing, D. H. Everett, R. A. W. Haul, L. Moscou, R. A. Pierotti, J. Rouquerol, and T. Siemieniowska, *Pure Appl. Chem.* **57**, 603 (1985).
- <sup>13</sup>J. C. P. Broekhoop and J. H. de Boer, *J. Catal.* **9**, 15 (1967).
- <sup>14</sup>S. Brunauer, P. H. Emmett, and E. Teller, *J. Am. Chem. Soc.* **60**, 309 (1938).
- <sup>15</sup>V. P. Parkhutik and V. I. Shershulsky, *J. Phys. D* **25**, 1258 (1992).
- <sup>16</sup>Y. Zhang, K. Yu, S. Ouyang, L. Luo, H. Hu, Q. Zhang, and Z. Zhu, *Physica B* **368**, 94 (2005).